1   **Chromosomal Resistance to Metronidazole in *Clostridioides difficile* can be**

2   **Mediated By Epistasis Between Iron Homeostasis and Oxidoreductases**

3

4   Aditi Deshpande[1#], Xiaoqian Wu[1#], Wenwen Huo[2,3], Kelli L. Palmer[2], Julian G. Hurdle[1]*

5   [1]Center for Infectious and Inflammatory Diseases, Institute of Biosciences and

6   Technology, Texas A&M Health Science Center, Houston, Texas 77030, USA.

7   [2]Department of Biological Sciences, University of Texas at Dallas, Richardson, TX

8   75080, USA.

9   [3]Department of Molecular Biology and Microbiology, Tufts University School of

10   Medicine, Boston, MA 02111, USA.

11

12   *Correspondence and requests for materials should be addressed to J.G.H

13   (jhurdle@tamu.edu).

14   #These authors equally contributed. Author order was determined both alphabetically

15   and in order of increasing seniority.

16

17   **Running title:** Metronidazole resistance in *C. difficile*

18   **Keywords:** Drug resistance evolution, redox stress, iron metabolism

19

20

21

22

23

24

1

Abstract

Chromosomal resistance to metronidazole has emerged in clinical *Clostridioides difficile*, but the genetic mechanisms remain unclear. This is further hindered by the inability to generate spontaneous metronidazole-resistant mutants in the lab to aid genetic studies. We therefore constructed a mismatch repair mutator, in non-toxigenic ATCC 700057, to unbiasedly survey the mutational landscape for *de novo* resistance mechanisms. In separate experimental evolutions, the mutator adopted a deterministic path to resistance, with truncation of ferrous iron transporter FeoB1 as a first-step mechanism of low level resistance. Allelic deletion of *feoB1* in ATCC 700057 reduced intracellular iron content, appearing to shift cells toward flavodoxin-mediated oxidoreductase reactions, which are less favorable for metronidazole's cellular action. Higher level resistance evolved from sequential acquisition of mutations to catalytic domains of pyruvate-ferredoxin oxidoreductase (PFOR encoded by *nifJ*); a synonymous codon change to *xdhA1* (xanthine dehydrogenase subunit A), likely affecting its translation; and lastly, frameshift and point mutations that inactivated the iron-sulfur cluster regulator (IscR). Gene silencing of *nifJ*, *xdhA1* or *iscR* with catalytically dead Cas9 revealed that resistance involving these genes only occurred when *feoB1* was inactivated i.e. resistance was only seen in an *feoB1*-deletion mutant and not the isogenic wild-type parent. These findings show that metronidazole resistance in *C. difficile* is complex, involving multi-genetic mechanisms that could intersect with iron-dependent metabolic pathways.

INTRODUCTION

Clostridioides difficile infection (CDI) is a leading cause of diarrhea in hospitalized patients in developed countries. Since 2003, the emergence and spread of epidemic strains has significantly increased the incidence and severity of CDI. The health care impact of the epidemic *C. difficile* strains is evident from there being about half a million cases of CDI and ~29,000 deaths in the United States in 2011 (1, 2).

Owing to its potent anti-anaerobic activity and low cost, metronidazole was traditionally preferred to treat mild to moderate CDI (3). Metronidazole is a 5-nitroimidazole prodrug that is primarily activated in anaerobes conducting reactions that generate low redox potentials (4). Enzymatic reduction of metronidazole occurs via reactions catalyzed by oxidoreductases, such as pyruvate-ferredoxin oxidoreductase (PFOR), and involves the transfer of electrons to its nitro group from cofactors like ferredoxin and flavodoxin. This produces an unstable nitroimidazole anion that may be converted to reactive desnitro, nitroso and hydroxylamine intermediates, which react with DNA, proteins and non-protein thiols to form adducts (4).

The efficacy of metronidazole has declined with the emergence of epidemic strains. Therefore, in the 2017 IDSA/SHEA treatment guidelines, metronidazole is no longer a first-line drug for adult CDI (5). However, there is a need for scientific evidence explaining the decline in metronidazole efficacy, as continued use of the drug is likely until the new guidelines become standard practice. The decline in metronidazole efficacy appears to correlate with the emergence and spread of resistant strains of different ribotype backgrounds (6-8); metronidazole resistance is defined by the EUCAST breakpoint of >2 µg/ml. For example, Snydman reported that ~8% of U.S.

70   isolates (2011-2016) are resistant to metronidazole (7), while the rate in Europe ranged

71   from 0.1% to 0.5% for isolates collected between 2011 to 2014 (6).

72   The foremost attempt to characterize the genetic basis for chromosomal

73   metronidazole resistance in a clinical strain was by Lynch *et al.* (9). The patient isolate

74   strain was isolated on metronidazole-containing agar, but was then passaged, *in vitro,*

75   in drug and was found to contain mutations in PFOR, ferric uptake regulator (Fur) and

76   the oxygen-independent coproporphyrinogen III oxidase (HemN) among other changes.

77   In another study, Moura *et al.* evaluated a non-toxigenic metronidazole-resistant *C.*

78   *difficile* showing it adjusted metabolic pathways that are linked to PFOR activity (10).

79   Most recently, Boekhoud *et al.* (11) reported that *C. difficile* clinical isolates carried a

80   conjugative plasmid (pCD-METRO) conferring resistance to metronidazole, but the

81   plasmid was not present in several CDI associated ribotypes that were metronidazole-

82   resistant. This indicates that pCD-METRO is not a universal mechanism of resistance;

83   furthermore, the genetic determinants on pCD-METRO directly responsible for the

84   phenotype are still unknown. Taken together, it appears *C. difficile* could have multiple

85   ways to evolve metronidazole resistance, but these mechanisms remain unclear or

86   require genetic and biochemical validation in naïve hosts. In contrast, mechanisms of

87   MTZ resistance in several pathogens for which the drug is prescribed are known e.g.

88   *Helicobacter pylori* and *Entamoeba* histolytica (4).

89   There have been two critical barriers to knowledge of metronidazole resistance

90   in *C. difficile*. Firstly, metronidazole-resistant mutants are designated to be unstable, as

91   evident by inconsistent metronidazole susceptibility profiles of the strains (9, 12).

92   Secondly, there is an inability to select laboratory mutants to allow for controlled genetic

93   studies (13). To address these challenges, from a laboratory perspective, we

94   constructed a mutator tool by deleting the DNA mismatch repair system in a non-

95   toxigenic *C. difficile* strain. Mutators are employed for accelerated evolution to study

96   mutation accumulation in bacteria (14, 15). Using this concept, we investigated the

97   genomic landscape of *C. difficile* for *de novo* resistance mechanisms that are

98   evolutionarily feasible, albeit *in vitro*. Hence, we obtained new insights that *C. difficile*

99   can manipulate iron uptake and iron-dependent oxidoreductive pathways to develop

100 resistance to metronidazole.

101

102 **RESULTS AND DISCUSSION**

103 **Hypermutator construction by deleting DNA mismatch repair (MMR) genes.** The

104 MutSL MMR proteins are involved in correcting replicative errors (16), wherein MutS

105 identifies mispaired or unpaired bases and recruits the endonuclease MutL that initiates

106 the removal and repair of misincorporated bases (16). *C. difficile* was found to carry

107 adjacent *mutS* and *mutL* genes (CD630_19770 and CD630_19760), in addition to the

108 *mutS* homolog *mutS2* (CD630_07090). To construct a *C. difficile* mutator, we chose the

109 strain ATCC 700057 (17) because it is non-pathogenic, lacking the toxin genes *tcdA*

110 and *tcdB* (18), and is widely used for antibiotic susceptibility testing (12). We individually

111 deleted *mutS*, *mutL*, *mutS2* and the entire *mutSL* operon by allelic exchange using

112 pMTL-SC7215; deletions were confirmed by PCR (19). Mutability was assessed from

113 the frequency of isolating mutants to the antibiotics rifaximin and fidaxomicin at 4 x their

114 MICs (0.5 and 0.25 μg/ml, respectively). As shown in **Fig. 1A** mutation frequencies were

115 enhanced upon deletion of *mutS* or *mutL*, but *mutS2* had no effect. Deletion of *mutSL*

116   caused the highest increase (>80-fold) in mutability with respect to WT ATCC 700057

117   i.e. mutation frequencies were 10^{-6} for 700057Δ*mutSL* versus 10^{-8} for the WT ATCC

118   700057; and this strain was significantly more mutable than Δ*mutS* or Δ*mutL* strains, as

119   determined by unpaired t-tests (**Table S1**). Mutability was reversed when

120   700057Δ*mutSL* was complemented with WT *mutSL* (**Fig. S1**). Thus, 700057Δ*mutSL*

121   (i.e. mutator) was used to select metronidazole-resistant mutants below.

122

123   **Experimental evolution of metronidazole resistance.** The agar MICs of

124   metronidazole against the WT and mutator was 0.25 μg/ml. However, spontaneous

125   mutants could not be selected by plating >10 overnight cultures of each strain onto

126   agars containing 2 and 4 x MICs (*data not shown*). Both strains were therefore serially

127   passaged on agars containing varying concentrations of metronidazole (0.125-16

128   μg/ml); each passage was incubated up to 3 days to obtain growth. In the first

129   experimental evolution, by the 9th passage, the mutator evolved resistance as its

130   population was inhibited by 2 μg/ml (**Fig. 1B**). By the 15th passage, the population was

131   inhibited at 8 μg/ml. In contrast, stable mutants did not arise from the WT ATCC

132   700057, even up to 15 serial passages in drug (**Fig. 1B**) and is consistent with prior

133   reports of an inability to isolate *in vitro* metronidazole-resistant mutants of *C. difficile*

134   (13). To further comprehend the evolutionary path to resistance, we conducted a

135   separate experimental evolution with the mutator and identified that by the 6th and 17th

136   passages the population was inhibited by 2 and 16 μg/ml of drug, respectively (**Fig. 1B,**

137   **C**).

138

6

Identification of genetic changes associated with *de novo* metronidazole resistance. As expected, the mutator accumulated insertions, substitutions and deletions across the genome and showed no genomic site specificity (**Fig. S2**). Functional gene classification showed that mutations occurred to iron transporters, iron-sulfur proteins, oxidoreductases, carbohydrate metabolism, fatty acid metabolism, cell surface/ division proteins and other genes (**Fig. S3**). However, to study mutations associated with resistance, we focused on proteins involved in cellular redox and metal homeostasis that may affect the activation of metronidazole.

(i) Identification of genetic changes in evolution 1. From the culture population at the endpoint of the evolution experiment 1 (passage 15), we isolated and genome sequenced three mutant colonies, designated as JWD-1 (MIC=8 μg/ml), JWD-2 (MIC=32 μg/ml) and JWD-3 (MIC=32 μg/ml). They all carried a frameshifting deletion (Glu38*fs*) in the FeoB1, encoded by CD630_14790; a substitution in PFOR (Gln$_{803}$Arg) encoded by *nifJ* (CD630_26820); and a synonymous change (AA**G**$_{2070}$AA**A**) in xanthine dehydrogenase subunit *xdhA1*, encoded by CD630_20730. JWD-2 and JWD-3 also carried unique changes of Lys$_{51}$*fs* and Val$_{76}$Ala respectively in the iron-sulfur cluster regulator (IscR), encoded by CD630_12780. These mutations in IscR may explain why JWD-2 and JWD-3 were 4-fold more resistant to metronidazole than JWD-1, which lacked changes to the regulator. We identified the order in which mutations arose (**Fig. 1C**) by determining the MICs and Sanger sequencing of three individual mutant colonies each from passages 10 and 13. Mutants from passage 10 had MICs of 2 μg/ml and carried the above variations in PFOR and FeoB1, while mutants (MICs of 8 μg/ml) from passage 13 also carried the synonymous change in *xdhA1*.

7

162   *(ii) Identification of genetic changes in evolution 2.*   JWD-4 (MIC=64 μg/ml), an

163   endpoint mutant (passage 17) of experiment 2 was isolated and genome sequenced.

164   Similar to the above endpoint mutants, JWD-4 contained disruptions to FeoB1 (Glu$_{40}$*fs*),

165   PFOR (Pro$_{32}$Leu) and IscR (Lys$_{51}$*fs*), but also acquired a Gly$_{270}$Asp substitution in

166   xanthine permease (CD630_20910). The order in which mutations arose (**Fig. 1C**) were

167   also determined by MIC testing and Sanger sequencing of minimum three colonies per

168   time point and metronidazole MICS were also measured. This revealed FeoB1 was

169   disrupted by passage 4 (MIC=1 μg/ml); PFOR by passage 7 (MIC=2 μg/ml); xanthine

170   permease by passage 14 (MIC=16 μg/ml); and IscR by passage 17 (MIC=64 μg/ml).

171   The occurrence of similar genetic changes in the two independent serial passage

172   experiments suggests there was a deterministic path to metronidazole resistance.

173

174   **Explanation of *de novo* genetic variations associated with metronidazole**

175   **resistance.**

176   *(i) FeoB1 participation.* Under anaerobic conditions, iron mostly exists in ferrous (Fe^{2+})

177   form. In *C. difficile,* FeoB1 is predicted to be the main iron transporter, as it is the most

178   upregulated iron transporter in low iron conditions and *in vivo* in hamsters (20, 21). *In*

179   *vitro*, the homologs FeoB2 and FeoB3 are thought to be less responsive to changes in

180   iron (20). Thus, the loss of FeoB1 may have lowered the supply of iron to iron carrier

181   proteins that mediate electron transfer to metronidazole (22). In support of our findings,

182   deletion of *feoAB* in *B. fragilis* conferred a 10-fold decrease in metronidazole activity

183   (23).

184

185   ***(ii) Oxidoreductases PFOR and XDH participation.*** PFOR catalyzes the oxidation of

186   pyruvate to acetyl-CoA, while XdhA1 is the molybdenum-binding subunit of xanthine

187   dehydrogenase (XDH) that catalyzes the oxidation of purines. Sequence alignment of

188   PFOR homologs of *C. difficile* (CD630_26820) *and Desulfovibrio africanus*

189   (Desaf_2186) (59.4% similarity) indicated that the $Pro_{32}Leu$ substitution occurred

190   adjacent to the critical threonine-31 site that forms the catalytic domain for pyruvate

191   binding, whereas $Gln_{803}Arg$ occurred in domain VI upstream of cysteine-815 that binds

192   the proximal [4Fe-4S] cluster (24, 25) (**Fig. S4**). These substitutions likely affected the

193   enzyme's catalytic activity, involving electron transfer to electron carrier proteins. To

194   evaluate the synonymous change in *xdhA1*, we analyzed its secondary structure using

195   the RNA folding algorithm mfold (26) to gauge potential effects on RNA translation. The

196   AA**G**$_{2070}$AA**A** change (**Fig. S5**) was predicted to introduce an unstable stem loop, with a

197   positive free energy change (ΔG = 3.8 kcal/mol for the mutant and ΔG = -25.9 kcal/mol

198   for the WT), which is unfavorable for RNA translation (27). With regard to xanthine

199   permease, the role of this transporter in metronidazole resistance is presently unclear,

200   although we speculate that $Gly_{270}Asp$ substitution might affect the supply of xanthine to

201   XDH.

202   ***(iii) IscR participation.*** Iron-sulfur [Fe–S] clusters are essential to the biochemistry of

203   several proteins that conduct electron transfer reactions (28, 29). In pathogenic bacteria

204   the assembly and incorporation of [Fe–S] clusters is mostly controlled by the *isc* and *suf*

205   operons, of which *isc* is the house-keeping system; furthermore, *C. difficile* lacks the *suf*

206   operon (30). Holo-IscR binds DNA as a homodimer, but damage to its [4Fe-4S] by

207   reactive free radicals or iron-starvation increases cellular levels of apo-IscR, triggering

208   defensive mechanisms including antioxidants such as cysteine and non-protein thiols

209   (31). The Lys51*fs* variation, in strains JWD-2 and JWD-4, disabled the function of IscR,

210   by forming an aberrant protein lacking cysteines-92, 98 and 104 that are required to

211   bind [4Fe-4S] (32). To characterize the effect of the $Val_{76}Ala$ substitution in IscR in

212   JWD-3, we analyzed the crystal structure of dimeric IscR bound to DNA from *E. coli*

213   (pdb ID: 4CHU) using UCSF Chimera (33). The IscRs from *C. difficile* ATCC 700057

214   and *E. coli* K12 are closely related with ~41% identical amino acids and valine-76 is a

215   conserved amino acid. In the dimeric structure (**Fig. S6**), valine-76 on Chain A occurs

216   with other lipophilic residues in a dimer interface where it hydrophobically interacts with

217   leucine-113 on Chain B. It is plausible that the less hydrophobic alanine-76 reduces

218   hydrophobic steric packing for stabilizing the dimeric DNA binding conformation of IscR.

219

220   **FeoB1-mediated cellular changes associated with metronidazole resistance**.

221   *(i) Deleting feoB1 affects resistance and iron-content.* Since *feoB1* was inactivated

222   early in the serial evolution (**Fig. 1C**), we first examined the role of this gene by deleting

223   it in ATCC 700057. The deletion mutant (700057*ΔfeoB1*) grew in 0.5 μg/ml of

224   metronidazole (MIC=1 μg/ml), whereas the WT strain grew in 0.125 μg/ml (MIC=0.25

225   μg/ml) of drug (**Fig. 2A**). Susceptibility was restored by complementing the *ΔfeoB1*

226   strain with WT *feoB1*, expressed from its own promoter in pMTL84151 (**Fig. 2A**). There

227   was ~21% lesser iron content in the mutant (0.0753 ± 0.002 ppm) compared to the WT

228   (0.0956 ± 0.004 ppm), as determined by ICP-OES. Consistent with reduced intracellular

229   iron content, 700057*ΔfeoB1* also showed increased transcription of *fur* (3.9 ± 0.17-fold)

230   and ferrichrome ABC transporter subunit (*fhuB*) (5.13 ± 0.25-fold), compared to the WT,

10

231   in the absence of drug (**Fig. 2B**). In drug, the Δ*feoB1* mutant showed 10.50 ± 0.96 (*fur*)

232   and 9.16 ± 0.25 (*fhuB*) fold higher gene expression than the WT (**Fig. 2B**).

233

234   ***(ii) Effect on expression of cofactors that activate metronidazole.*** Since the loss of

235   *feoB1* reduced iron content in cells, we reasoned this may diminish metronidazole

236   activation by limiting iron-dependent electron carrier proteins such as ferredoxins.

237   Ferredoxin and flavodoxin are small redox proteins that accept and transfer electrons to

238   metronidazole from oxidoreductases, such as PFOR. Transcriptional analysis revealed

239   that in the absence of drug, 700057Δ*feoB1* downregulated (-2.46 ± 0.09-fold) the

240   ferredoxin (*fdx* i.e. CD630_06271) and upregulated (2.04 ± 0.06-fold) the flavodoxin

241   (*fldx* i.e. CD630_19990) relative to WT (**Fig. 2C**). When 700057Δ*feoB1* was exposed to

242   metronidazole, there was further downregulation of *fdx* (-7.51 ± 0.21-fold) and

243   upregulation of *fldx* (6.860 ± 0.43-fold) (**Fig. 2C**). Other ferredoxin and flavodoxin

244   homologs (**Fig. S7**) were lesser expressed supporting published studies that

245   CD630_06271 and CD630_19990 are the most responsive homologs of ferredoxin and

246   flavodoxin, during iron stress in *C. difficile* (20, 21). Ferredoxin is better at transferring

247   electrons to metronidazole, due to carriage of an iron-sulfur cluster that has a lower

248   redox potential than flavodoxin, which carries flavin mononucleotide (34). Thus, these

249   results indicate that loss of *feoB1* led to reduced iron content, prompting a shift to

250   flavodoxin-mediated oxidoreductase reactions that enable cells to resist metronidazole.

251

252   ***(iii) Effect on cellular accumulation of nitroimidazole.*** Since the above results

253   suggest the loss of *feoB1* might decrease metronidazole activation, we quantified the

11

254 intracellular concentration of dimetridazole, a related nitroimidazole (35). Dimetridazole

255 was used due to the commercial availability of 5-amino-1,2-dimethylimidazole, a likely

256 end-product of dimetridazole activation (35) that could be used as a standard in the LC-

257 MS/MS. Against dimetridazole, 700057Δ*feoB1* showed the same level of resistance to

258 metronidazole (i.e. MIC=1 μg/ml). Concentrated cells were exposed to 1 mM of

259 dimetridazole for 1 hour and intracellular concentrations measured in cell lysates. In

260 700057Δ*feoB1*, there was 7.31 ± 0.53 μM of dimetridazole (**Fig. 2D**), which represents

261 about 34% lower intracellular drug accumulation, compared to the WT (11.07 ± 1.26

262 μM). The accumulation of metronidazole and other nitroimidazoles into bacteria is

263 thought to occur in a concentration-dependent manner, whereby as the drug is activated

264 in cells more drug is taken up (36). Thus, the observed lower intracellular accumulation

265 of dimetridazole in 700057Δ*feoB1* might indicate lesser drug activation, which could be

266 expected with a shift to flavodoxin-mediated metabolism. However, we could not detect

267 the amine end-product, which would have provided a measure of drug activation.

268

269 **Resistance mediated by *nifJ*, *xdhA1* and *iscR* appear to require the loss of *feoB1*.**

270 To assess the roles played by *nifJ*, *xdhA1* and *iscR* in metronidazole resistance, we

271 silenced these genes using a xylose-inducible CRISPR-interference vector. In this

272 approach, fusion of antisense nucleotides to the guide RNA of Cas9 blocks gene

273 transcription (37) and is a more facile approach than gene deletions in *C. difficile*. As a

274 positive control, an antisense to *feoB1* was included to measure the effect of gene

275 silencing on growth in metronidazole. Even though gene silencing reduced transcript

276 levels by ~10-fold (**Fig. 3A**), resistance was only detected in the strain expressing the

277   *feoB1* antisense (MIC = 1 μg/ml); the strain carrying the empty vector was inhibited by

278   0.25 μg/ml (**Fig. 3B**). Given that *feoB1* mutants arose early in the passages (**Fig. 1C**,

279   we therefore questioned whether expression of resistance involving *nifJ*, *xdhA1* or *iscR*

280   required the loss of *feoB1*. As shown in **Fig. 3C**, the abovementioned antisenses

281   enhanced survival of 700057Δ*feoB1*, shifting MICs to 8 μg/ml. Thus, the loss of *feoB1*

282   early in the serial evolution, might have influenced the direction of resistance evolution

283   toward genes that when disrupted took advantage of lower iron content (i.e.

284   combinatorial or epistatic resistance).

285   To confirm that combinatorial resistance was more protective, we exposed cells

286   to 8 μg/ml of metronidazole and analyzed effects on DNA integrity, non-protein thiols

287   and transcription of redox-responsive genes (38, 39). The combinatorial-resistant

288   strains showed more intact DNA, while damage was seen to the DNA of 700057Δ*feoB1*,

289   but was more marked in WT strain (**Fig. 4A**). Likewise, there were higher amounts of

290   free-non-protein thiols in combinatorial-resistant strains (**Fig. 4B**), suggesting a decline

291   in formation of covalent adducts with activated metronidazole. Combinatorial-resistant

292   strains also showed reduced transcription of the DNA damage response gene *recA*

293   (CD630_13280); and redox stress responsive genes (hybrid cluster protein,

294   CD630_21680 and thioredoxin A, CD630_30330) (**Fig. 4C**). Taken together, these

295   results confirm the role of *feoB1* in the evolution of a novel epistatic mechanism of

296   metronidazole resistance. Epistatic mechanisms of antimicrobial resistance are also

297   seen in fluoroquinolone-resistant *E. coli*, with double mutations to gyrase A and

298   topoisomerase IV, which produce high-level resistance that is greater than predicted

299   from individual mutations (40).

300

301 **Further assessment of the function of IscR in resistance.** As IscR has not been

302 previously linked to metronidazole resistance, we further investigated its role by

303 focusing on pyruvate-lactate metabolism that is affected by iron-sulfur metabolism and

304 is indicative of metronidazole resistance in *B. fragilis* (41). Depletion of *iscR* mRNA in

305 700057Δ*feoB1* further diminished the transcription of *nifJ* (-6.17 $\pm$ 0.29-fold), which was

306 already marginally reduced (-2.67 $\pm$ 0.18-fold) with the loss *of feoB1* in 700057Δ*feoB1*

307 compared to WT (**Fig. 5A**). The strain bearing the *iscR* antisense also showed

308 increased levels of pyruvate (1.33 $\pm$ 0.03 nM) and lactate (1.86 $\pm$ 0.08 nM) compared

309 the parent 700057Δ*feoB1* (0.98 $\pm$ 0.02 nM and 1.13 $\pm$ 0.045 nM respectively) (**Fig. 5B**).

310 This can be expected if downregulation of *nifJ* further reduced the levels of PFOR

311 protein in cells, which would concomitantly decrease metronidazole activation by the

312 enzyme. Furthermore, a reduction in PFOR activity may also drive the conversion of

313 pyruvate to lactate via lactate dehydrogenase. Therefore, it appears that loss of *iscR* at

314 the endpoint of the evolution (**Fig. 1C**) affected iron-sulfur dependent electron transfer

315 reactions and synergized with both the loss of *feoB1* and mutated oxidoreductase

316 enzymes, which occurred at the earlier evolutionary steps. To confirm the hypothesis

317 that loss of *iscR* affected electron transfer reactions, we tested the susceptibility of cells

318 to the electron acceptor plumbagin, a naphthoquinone that is reduced in reactions

319 catalyzed by oxidoreductases (42). In *Xanthomonas campestris,* the loss of iscR led to

320 plumbagin resistance (43). Our results show that WT ATCC 700057 was inhibited by

321 0.5 µg/ml of plumbagin, while moderate resistance was seen in 700057Δ*feoB1* (MIC=2

322 µg/ml). Depletion of *iscR* mRNA in 700057Δ*feoB1* further elevated resistance to

14

323   plumbagin (MIC=8 μg/ml), in a manner analogous to above observations for

324   metronidazole (**Fig. 5C**).

325

326   **CONCLUSION**

327   The involvement of mutations to multiple genes might partly explain why *C. difficile* was

328   slow to evolve chromosomal resistance to metronidazole, in spite of the drug being

329   used since 1980s. While mutations to *feoB1* and oxidoreductases are known to

330   individually cause metronidazole resistance in other organisms (4), to the best of our

331   knowledge there are no reports of epistatic interactions between these mechanisms.

332   Nonetheless, our results generated a model (**Fig. 6**) of metronidazole resistance that

333   could help interpret genetic changes seen in *C. difficile* clinical isolates, which lack pCD-

334   METRO (11). For example, our model in **Fig. 6** generally explains the mechanism of

335   mutations seen a metronidazole-resistant NAP1 *C. difficile* (9, 44); in that study, the

336   strain had mutations to Fur and PFOR ($Gly_{423}Glu$). Disruption of Fur might have affected

337   iron homeostasis to reduce drug susceptibility, which is also shown in *H. pylori* (45).

338   Similarly, the amino acid change in PFOR occurred in domain III, an important subunit

339   for binding of the coenzyme A substrate (25). However, we recognize that FeoB1 is

340   essential for colonization and virulence in other bacteria, which makes it improbable that

341   *C. difficile* will inactivate *feoB1 in vivo* during metronidazole therapy. This raises an

342   important question of whether there are lower free iron concentrations in the

343   gastrointestinal tract that may provide a milieu for resistance to be exhibited by strains

344   with mutated oxidoreductases such as PFOR. Conversely, such resistant strains could

345   be difficult to detect, as current susceptibility testing methods for *C. difficile* use iron-rich

15

346   medium, and may be categorized as susceptible. Indeed, ineffective detection of

347   metronidazole-resistant *C. difficile* has also been a major concern (9, 12).

348   A number of outstanding questions remain concerning the apparent multi-genetic

349   mechanisms of metronidazole resistance. Certainly, it is important to establish which

350   resistance mechanisms do or do not impose physiological costs, as this factor might

351   influence the future clinical prevalence of strains. There is also a need to identify

352   whether there are metronidazole-resistant *C. difficile* that also resist oxidative stress, as

353   is known in metronidazole-resistant *H. pylori* and *E.* histolytica that upregulate

354   superoxide dismutase (46, 47). Therefore, in the aftermath of metronidazole use for

355   adult CDI, studies are still warranted to assess the extent to which metronidazole

356   resistance could shape *C. difficile* evolution, epidemiology and pathophysiology.

357

358   **MATERIALS AND METHODS**

359   **Strains and culture conditions**. Non-toxigenic *C. difficile* ATCC 700057 and derivative

360   strains were routinely grown in pre-reduced Brain Heart Infusion (BHI) broth or agar at

361   37°C in a Whitley A35 anaerobic workstation (Don Whitley Scientific). *Escherichia coli*

362   strains NEB 5-alpha, CA434 and SD46 were grown at 37°C in LB broth or agar. All

363   strains and plasmids used in this study are listed in **Table S2**. D-cycloserine (250

364   μg/ml), cefoxitin (8 μg/ml), and thiamphenicol (15 μg/ml) were used to selectively culture

365   *C. difficile* containing plasmids, whereas chloramphenicol (15 μg/ml) and ampicillin (50

366   μg/ml) or kanamycin (50 μg/ml) were used to grow *E. coli* SD46 and CA4343

367   respectively. Wherever needed, data was normalized to the protein content.

368

16

369   **Antimicrobial susceptibility**. Agar MICs were determined on BHI agar supplemented

370   with hemin (5 μg/ml) and used an inocula of 10^5 CFU/ml. Agars contained doubling

371   dilutions of compound from 0.06 to 64 μg/ml.

372

373   **Genetic manipulation of *C. difficile***. The vector pMTL-SC7215 was used to delete

374   target genes in *C. difficile* by allelic exchange (19). Allelic exchange vectors to delete

375   *mutS, mutS2, mutSL, mutL* and *feoB1* were conjugated into *C. difficile* via *E. coli* donor

376   strains (CA434 or SD46). Allelic exchange was conducted as described (19).

377   Successful gene knockouts were confirmed by PCR. For complementation, *feoB1* was

378   synthesized and cloned into XmaI and XbaI sites of the vector pMTL-84151 by

379   Genscript. Primers used in the study are in **Table S3**. The designed allelic cassettes

380   used in this study are described in the supplementary **Table S4.**

381

382   **Gene knockdown.** The xylose-inducible vector pXWpxyl-*dcas9* was used to silence

383   the transcription of *feoB1, nifJ*, *iscR* and *xdhA1*, as previously described (37). The

384   sgRNA (**Table S5**) targeting the abovementioned genes were synthesized and cloned

385   into the vector's PmeI site by Genscript Biotech (New Jersey). Antisenses were induced

386   with 2% w/v of xylose.

387

388   **Determination of mutation frequencies**. Briefly, *C. difficile* strains were grown

389   overnight in BHI broth, centrifuged and concentrated 10-fold. Aliquots (0.1 ml) of each

390   culture were plated onto pre-reduced BHI agar plates containing 0.32 μg/ml fidaxomicin

391   or 0.5 μg/ml rifaximin, representing 4 x MICs. Similarly, WT and mutator cultures (>10

17

392   each) were concentrated and plated onto agar plates containing 2 or 4 x MIC (i.e. 0.5 or

393   1 μg/ml of metronidazole). After 48 hours of incubation, the mutation frequencies were

394   calculated as the number of resistant colonies divided by total viable counts.

395

396   **Experimental evolution by serial passaging.** From an overnight culture on agar, *C.*

397   *difficile* colonies were resuspended into 1 ml of BHI broth to produce an optical density

398   of OD_{600}nm of ~0.8-1.0. At each passage step, an aliquot of 0.01 ml (inocula of 10^5-10^6

399   CFU/mL) was spread onto BHI agars containing 0.25 to 64 × MIC of metronidazole.

400   After 48 to 72 hours of incubation, colonies were isolated from the highest concentration

401   permitting visible growth and were resuspended in fresh broth, before passaging the

402   suspension onto higher drug concentrations. The remaining was stored in glycerol.

403

404   **Genome sequencing and analysis.** Whole genome sequencing was done by paired

405   end sequencing at SeqMatics LLC (California) and MRDNA (Texas). CLC Genomics

406   Workbench version 12 (Qiagen) was used to *de novo* assemble WT ATCC 700057. The

407   assembled genome of the WT was annotated using Rapid Annotation using Subsystem

408   Technology (RAST) [49] and was used for mapping the mutator 700057Δ*mutSL* and

409   metronidazole-resistant mutants (JWD-1, JWD-2, JWD-3 and JWD-4). Sequence

410   variations were identified using "Quality-based variant detection" tool in CLC Genomics

411   Workbench with default parameters (≥10-fold coverage of the reference position and

412   sequence variation ≥35% of mapped reads). Mutations detected in the endpoint

413   mutants, compared to the WT, were screened against the 700057Δ*mutSL* to remove

414   shared variations, to focus on those that arose during the evolutions. For confirmation,

415   the variations in ≥90% of mapped reads were further analyzed manually. The coverage

416   for each genomic location was calculated in the CLC software and zero coverage

417   regions were then identified using a customized perl script. Genetic changes were

418   confirmed by Sanger sequencing.

419   **Growth kinetics of genetically manipulated strains.** Two-fold serial dilutions of drugs

420   was made in sterile pre-reduced BHI broth and 2% sterile xylose was used to induce

421   antisense expression. Overnight grown cultures were diluted 1:100 and inocula (OD_{600}

422   ~0.3) was added to the pre-reduced 96 well plates and incubated in an anaerobic

423   chamber for 24 hours. Plates were read for $Absorbance_{600}$ using Synergy H1 Microplate

424   Reader (BioTek).

425

426   **Quantification of intracellular iron by ICP-OES.** Overnight grown cells were

427   subcultured (1:100) in fresh BHI broth and harvested after 6 h for ICP-OES analysis to

428   determine the cellular iron levels. Samples were washed twice, centrifuged at 5000 rpm

429   and air dried. Samples were first digested in a microwave at 250°C at an initial

430   pressure of 40 bar, at 250°C the pressure was about 80 bar. Precisely weighed samples

431   were loaded into the digestion tube and 4 ml 16N HNO_3 was added. After digestion,

432   concentrated HNO_3 was evaporated at 100°C, before addition of 5 ml 2% HNO_3 and

433   heating at 120°C to re-dissolve the samples. After weighing, iron content was

434   measured with Agilent 725 ICP-OES. Calibration curves were made using standard

435   solutions of iron at concentrations of 5 ppb-500 ppb.

436

437 **LC-MS/MS analysis of cellular lysates**. Ten-fold concentrated, logarithmically growing

438 cells (OD_{600} ~0.3) were exposed to dimetridazole 1 mM and samples were harvested

439 after 1 hour of incubation. Cellular lysates (10 μl) were mixed with methanol (90 μl),

440 vortexed and centrifuged at 15,000 x g for 10 min. Supernatant (5 μl) was injected on to

441 UHPLC-Q Exactive MS system for analysis. The concentration of dimetridazole was

442 calculated based on the standard curve; further details are found in the supplementary.

443

444 **Analysis of DNA damage**. Samples were harvested as above, after exposing to

445 metronidazole 8 μg/ml and DNA damage was analyzed by alkaline agarose gel

446 electrophoresis as described (48), except for the following changes. The lysis buffer

447 contained lysozyme (0.5 mg/ml) and the agarose plugs were incubated at 37° C for 4 h.

448 0.5% v/v of hydrogen peroxide was a positive control to assess DNA fragmentation.

449

450 **Quantification of non-protein thiols**. Samples harvested as above, were processed in

451 5% w/v trichloroacetic acid as previously described (38). Thiol content was then

452 measured using the Thiol Fluorescent Detection Kit (Invitrogen), according to the

453 manufacturer's instructions.

454

455 **Transcriptional analysis**. After harvesting the samples as above, bacterial

456 RNAprotect™ reagent (QIAGEN) was then added to cultures and RNA isolated using

457 Qiagen's RNeasy mini kit. RNA was converted to cDNA by M-MLV reverse

458 transcriptase (Quantabio) using qScript cDNA SuperMix. qScript One-Step SYBR

459 Green qRT-PCR Kit, ROX (Quantabio) and gene-specific primers were used to amplify

460   genes in Applied Biosystems ViiA7 real-time PCR machine. Transcript levels were

461   calculated by the comparative Ct Method (ΔΔCT method) and data normalized to 16S

462   rRNA.

463

464   **Quantification of lactate and pyruvate.** Samples were harvested as above; lactate

465   and pyruvate were detected using Pyruvate Colorimetric/Fluorometric Assay kit

466   (Biovison) and Lactate-Glo^{TM} Assay kit (Promega).

467

476

477

478   **REFERENCES**

479   1.   Lessa FC, Mu Y, Bamberg WM, Beldavs ZG, Dumyati GK, Dunn JR, Farley MM,

480   Holzbauer SM, Meek JI, Phipps EC, Wilson LE, Winston LG, Cohen JA, Limbago BM,

481   Fridkin SK, Gerding DN, McDonald LC. 2015. Burden of *Clostridium difficile* infection in

482   the United States. N Engl J Med 372:825-34.

483   2.   Freeman J, Bauer MP, Baines SD, Corver J, Fawley WN, Goorhuis B, Kuijper EJ, Wilcox

484   MH. 2010. The changing epidemiology of *Clostridium difficile* infections. Clin Microbiol

485   Rev 23:529-49.

486   3.   Pelaez T, Alcala L, Alonso R, Rodriguez-Creixems M, Garcia-Lechuz JM, Bouza E.

487   2002. Reassessment of *Clostridium difficile* susceptibility to metronidazole and

488   vancomycin. Antimicrob Agents Chemother 46:1647-50.

489   4.   Dingsdag SA, Hunter N. 2018. Metronidazole: an update on metabolism, structure-

490   cytotoxicity and resistance mechanisms. J Antimicrob Chemother 73:265-279.

491   5.   McDonald LC, Gerding DN, Johnson S, Bakken JS, Carroll KC, Coffin SE, Dubberke

492   ER, Garey KW, Gould CV, Kelly C, Loo V, Shaklee Sammons J, Sandora TJ, Wilcox

493   MH. 2018. Clinical Practice Guidelines for *Clostridium difficile* Infection in Adults and

494   Children: 2017 Update by the Infectious Diseases Society of America (IDSA) and

495   Society for Healthcare Epidemiology of America (SHEA). Clin Infect Dis 66:e1-e48.

496   6.   Freeman J, Vernon J, Pilling S, Morris K, Nicholson S, Shearman S, Longshaw C,

497   Wilcox MH, Pan-European Longitudinal Surveillance of Antibiotic Resistance among

498   Prevalent *Clostridium difficile* Ribotypes Study G. 2018. The ClosER study: results from

499   a three-year pan-European longitudinal surveillance of antibiotic resistance among

500   prevalent *Clostridium difficile* ribotypes, 2011-2014. Clin Microbiol Infect 24:724-731.

501   7.   Thorpe CM, McDermott LA, Tran MK, Chang J, Jenkins SG, Goldstein EJC, Patel R,

502   Forbes BA, Johnson S, Gerding DN, Snydman DR. 2019. U.S.-Based National

22

503   Surveillance for Fidaxomicin Susceptibility of *Clostridioides difficile*-Associated Diarrheal

504   Isolates from 2013 to 2016. Antimicrob Agents Chemother 63.

505   8.   Adler A, Miller-Roll T, Bradenstein R, Block C, Mendelson B, Parizade M, Paitan Y,

506   Schwartz D, Peled N, Carmeli Y, Schwaber MJ. 2015. A national survey of the molecular

507   epidemiology of *Clostridium difficile* in Israel: the dissemination of the ribotype 027 strain

508   with reduced susceptibility to vancomycin and metronidazole. Diagn Microbiol Infect Dis

509   83:21-4.

510   9.   Lynch T, Chong P, Zhang J, Hizon R, Du T, Graham MR, Beniac DR, Booth TF, Kibsey

511   P, Miller M, Gravel D, Mulvey MR, Canadian Nosocomial Infection Surveillance P. 2013.

512   Characterization of a stable, metronidazole-resistant *Clostridium difficile* clinical isolate.

513   PLoS One 8:e53757.

514 10.   Moura I, Monot M, Tani C, Spigaglia P, Barbanti F, Norais N, Dupuy B, Bouza E,

515   Mastrantonio P. 2014. Multidisciplinary analysis of a nontoxigenic *Clostridium difficile*

516   strain with stable resistance to metronidazole. Antimicrob Agents Chemother 58:4957-

517   60.

518 11.   Boekhoud IM, Hornung BVH, Sevilla E, Harmanus C, Bos-Sanders I, Terveer EM, Bolea

519   R, Corver J, Kuijper EJ, Smits WK. 2020. Plasmid-mediated metronidazole resistance in

520   *Clostridioides difficile*. Nat Commun 11:598.

521 12.   Moura I, Spigaglia P, Barbanti F, Mastrantonio P. 2013. Analysis of metronidazole

522   susceptibility in different *Clostridium difficile* PCR ribotypes. J Antimicrob Chemother

523   68:362-5.

524 13.   Kumar M, Adhikari S, Hurdle JG. 2014. Action of nitroheterocyclic drugs against

525   *Clostridium difficile*. Int J Antimicrob Agents 44:314-9.

526 14.   Canfield GS, Schwingel JM, Foley MH, Vore KL, Boonanantanasarn K, Gill AL, Sutton

527   MD, Gill SR. 2013. Evolution in fast forward: a potential role for mutators in accelerating

528   *Staphylococcus aureus* pathoadaptation. J Bacteriol 195:615-28.

529 15. Long H, Miller SF, Strauss C, Zhao C, Cheng L, Ye Z, Griffin K, Te R, Lee H, Chen CC,
530   Lynch M. 2016. Antibiotic treatment enhances the genome-wide mutation rate of target
531   cells. Proc Natl Acad Sci U S A 113:E2498-505.

532 16. Lenhart JS, Pillon MC, Guarne A, Biteen JS, Simmons LA. 2015. Mismatch repair in
533   Gram-positive bacteria. Res Microbiol doi:10.1016/j.resmic.2015.08.006.

534 17. Leeds JA, Sachdeva M, Mullin S, Barnes SW, Ruzin A. 2014. In vitro selection, via serial
535   passage, of *Clostridium difficile* mutants with reduced susceptibility to fidaxomicin or
536   vancomycin. J Antimicrob Chemother 69:41-4.

537 18. Zhou Y, Mao L, Yu J, Lin Q, Luo Y, Zhu X, Sun Z. 2019. Epidemiology of *Clostridium*
538   *difficile* infection in hospitalized adults and the first isolation of *C. difficile* PCR ribotype
539   027 in central China. BMC Infect Dis 19:232.

540 19. Cartman ST, Kelly ML, Heeg D, Heap JT, Minton NP. 2012. Precise manipulation of the
541   *Clostridium difficile* chromosome reveals a lack of association between the tcdC
542   genotype and toxin production. Appl Environ Microbiol 78:4683-90.

543 20. Ho TD, Ellermeier CD. 2015. Ferric Uptake Regulator Fur Control of Putative Iron
544   Acquisition Systems in *Clostridium difficile*. J Bacteriol 197:2930-40.

545 21. Hastie JL, Hanna PC, Carlson PE. 2018. Transcriptional response of *Clostridium difficile*
546   to low iron conditions. Pathog Dis 76.

547 22. Yeom J, Imlay JA, Park W. 2010. Iron homeostasis affects antibiotic-mediated cell death
548   in *Pseudomonas* species. J Biol Chem 285:22689-95.

549 23. Veeranagouda Y, Husain F, Boente R, Moore J, Smith CJ, Rocha ER, Patrick S, Wexler
550   HM. 2014. Deficiency of the ferrous iron transporter FeoAB is linked with metronidazole
551   resistance in *Bacteroides fragilis*. J Antimicrob Chemother 69:2634-43.

552 24. Pieulle L, Magro V, Hatchikian EC. 1997. Isolation and analysis of the gene encoding the
553   pyruvate-ferredoxin oxidoreductase of *Desulfovibrio africanus*, production of the

24

554   recombinant enzyme in *Escherichia coli*, and effect of carboxy-terminal deletions on its

555   stability. J Bacteriol 179:5684-92.

556   25.   Chen PY, Aman H, Can M, Ragsdale SW, Drennan CL. 2018. Binding site for coenzyme

557   A revealed in the structure of pyruvate:ferredoxin oxidoreductase from *Moorella*

558   *thermoacetica*. Proc Natl Acad Sci U S A 115:3846-3851.

559   26.   Zuker M. 2003. Mfold web server for nucleic acid folding and hybridization prediction.

560   Nucleic Acids Res 31:3406-15.

561   27.   Digby WSaD. 1999. mRNAs have greater negative folding free energies than shuffled or

562   codon choice randomized sequences. Nucl Acid Research 27:1578-1584.

563   28.   Yeo WS, Lee JH, Lee KC, Roe JH. 2006. IscR acts as an activator in response to

564   oxidative stress for the suf operon encoding Fe-S assembly proteins. Mol Microbiol

565   61:206-18.

566   29.   Giel JL, Rodionov D, Liu M, Blattner FR, Kiley PJ. 2006. IscR-dependent gene

567   expression links iron-sulphur cluster assembly to the control of O2-regulated genes in

568   *Escherichia coli*. Mol Microbiol 60:1058-75.

569   30.   Andre G, Haudecoeur E, Courtois E, Monot M, Dupuy B, Rodionov DA, Martin-

570   Verstraete I. 2017. Cpe1786/IscR of *Clostridium perfringens* represses expression of

571   genes involved in Fe-S cluster biogenesis. Res Microbiol 168:345-355.

572   31.   Santos JA, Alonso-Garcia N, Macedo-Ribeiro S, Pereira PJ. 2014. The unique regulation

573   of iron-sulfur cluster biogenesis in a Gram-positive bacterium. Proc Natl Acad Sci U S A

574   111:E2251-60.

575   32.   Fleischhacker AS, Stubna A, Hsueh KL, Guo Y, Teter SJ, Rose JC, Brunold TC, Markley

576   JL, Munck E, Kiley PJ. 2012. Characterization of the [2Fe-2S] cluster of *Escherichia coli*

577   transcription factor IscR. Biochemistry 51:4453-62.

578   33.   Pettersen EF, Goddard TD, Huang CC, Couch GS, Greenblatt DM, Meng EC, Ferrin TE.

579   2004. UCSF Chimera--a visualization system for exploratory research and analysis. J

580   Comput Chem 25:1605-12.

581   34.   Guerlesquin MBaFo. 1988. Structure, function and evolution of bacterial ferredoxins.

582   FEMS Microbiology Reviews 54 155-176.

583   35.   Carlier JP, Sellier N, Rager MN, Reysset G. 1997. Metabolism of a 5-nitroimidazole in

584   susceptible and resistant isogenic strains of *Bacteroides fragilis*. Antimicrob Agents

585   Chemother 41:1495-9.

586   36.   Cudmore SL, Delgaty KL, Hayward-McClelland SF, Petrin DP, Garber GE. 2004.

587   Treatment of infections caused by metronidazole-resistant *Trichomonas vaginalis*. Clin

588   Microbiol Rev 17:783-93, table of contents.

589   37.   Marreddy RKR, Wu X, Sapkota M, Prior AM, Jones JA, Sun D, Hevener KE, Hurdle JG.

590   2019. The Fatty Acid Synthesis Protein Enoyl-ACP Reductase II (FabK) is a Target for

591   Narrow-Spectrum Antibacterials for *Clostridium difficile* Infection. ACS Infect Dis 5:208-

592   217.

593   38.   Leitsch D, Kolarich D, Wilson IB, Altmann F, Duchene M. 2007. Nitroimidazole action in

594   *Entamoeba histolytica*: a central role for thioredoxin reductase. PLoS Biol 5:e211.

595   39.   Leitsch D, Schlosser S, Burgess A, Duchene M. 2012. Nitroimidazole drugs vary in their

596   mode of action in the human parasite *Giardia lamblia*. Int J Parasitol Drugs Drug Resist

597   2:166-70.

598   40.   Huseby DL, Pietsch F, Brandis G, Garoff L, Tegehall A, Hughes D. 2017. Mutation

599   Supply and Relative Fitness Shape the Genotypes of Ciprofloxacin-Resistant

600   *Escherichia coli*. Mol Biol Evol 34:1029-1039.

601   41.   de Freitas MC, Resende JA, Ferreira-Machado AB, Saji GD, de Vasconcelos AT, da

602   Silva VL, Nicolas MF, Diniz CG. 2016. Exploratory Investigation of *Bacteroides fragilis*

603   Transcriptional Response during *In vitro* Exposure to Subinhibitory Concentration of

604   Metronidazole. Front Microbiol 7:1465.

605   42.   Imlay J, Fridovich I. 1992. Exogenous quinones directly inhibit the respiratory NADH

606   dehydrogenase in *Escherichia coli.* Arch Biochem Biophys 296:337-46.

607   43.   Fuangthong M, Jittawuttipoka T, Wisitkamol R, Romsang A, Duang-nkern J,

608   Vattanaviboon P, Mongkolsuk S. 2015. IscR plays a role in oxidative stress resistance

609   and pathogenicity of a plant pathogen, *Xanthomonas campestris.* Microbiol Res

610   170:139-46.

611   44.   Chong PM, Lynch T, McCorrister S, Kibsey P, Miller M, Gravel D, Westmacott GR,

612   Mulvey MR, Canadian Nosocomial Infection Surveillance P. 2014. Proteomic analysis of

613   a NAP1 *Clostridium difficile* clinical isolate resistant to metronidazole. PLoS One

614   9:e82622.

615   45.   Choi SS, Chivers PT, Berg DE. 2011. Point mutations in *Helicobacter pylori*'s fur

616   regulatory gene that alter resistance to metronidazole, a prodrug activated by chemical

617   reduction. PLoS One 6:e18236.

618   46.   Samarawickrema NA, Brown DM, Upcroft JA, Thammapalerd N, Upcroft P. 1997.

619   Involvement of superoxide dismutase and pyruvate:ferredoxin oxidoreductase in

620   mechanisms of metronidazole resistance in *Entamoeba histolytica.* J Antimicrob

621   Chemother 40:833-40.

622   47.   Tsugawa H, Suzuki H, Satoh K, Hirata K, Matsuzaki J, Saito Y, Suematsu M, Hibi T.

623   2011. Two amino acids mutation of ferric uptake regulator determines *Helicobacter pylori*

624   resistance to metronidazole. Antioxid Redox Signal 14:15-23.

625   48.   Zirkle RE, Krieg NR. 1996. Development of a method based on alkaline gel

626   electrophoresis for estimation of oxidative damage to DNA in *Escherichia coli.* J Appl

627   Bacteriol 81:133-8.

628

629

630   **FIGURES**

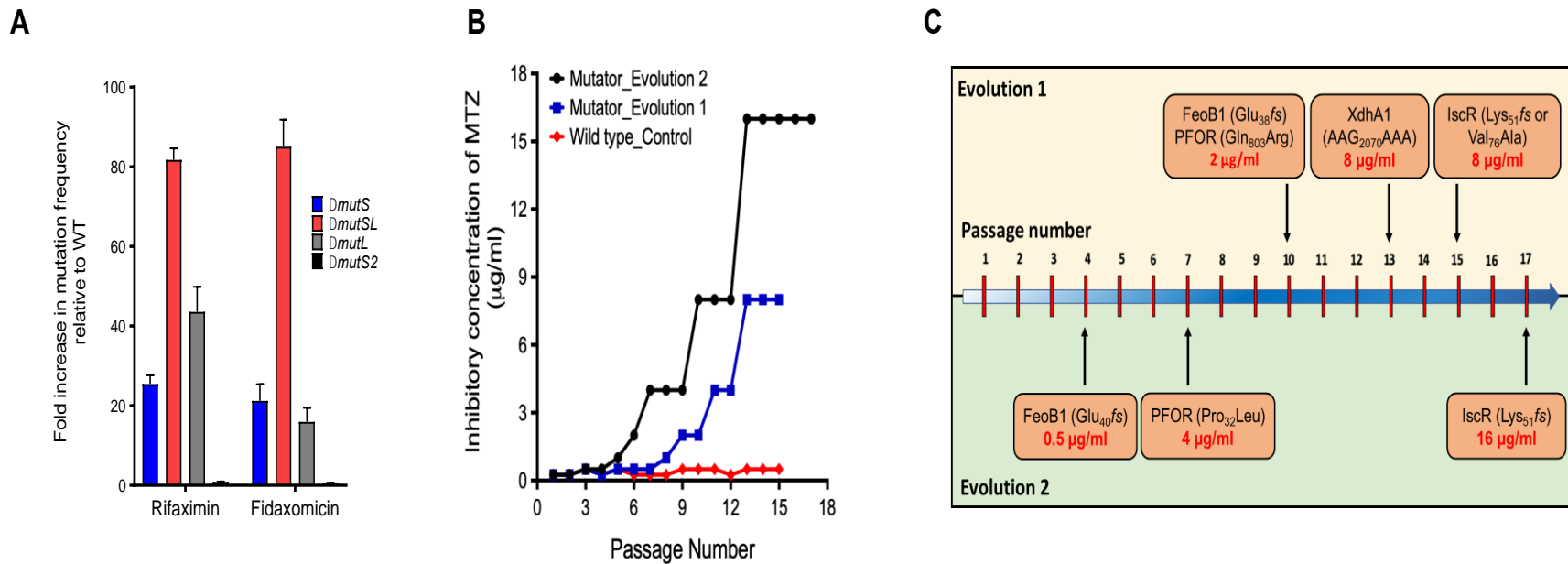631   Figures 1-6 are show below.

632

633

634

635

636

637

638

639

640

641

642

643

644

Figure 1. Evolution of metronidazole (MTZ) resistance using mismatch repair (MMR) deficient mutator. (**A**) Rifaximin and fidaxomicin mutation frequencies (MFs) of strains with deletions in MMR genes; fold change in MFs are relative to WT ATCC 700057. Plotted are means ± SEM from three biological replicates. (**B**) Two independent experimental evolutions with the mutator (Δ*mutSL*) resulted in MTZ-resistant mutants, in contrast to the WT. (**C**) The order in which mutation were accumulated in the two evolutions suggest there was a deterministic path to resistance.

654
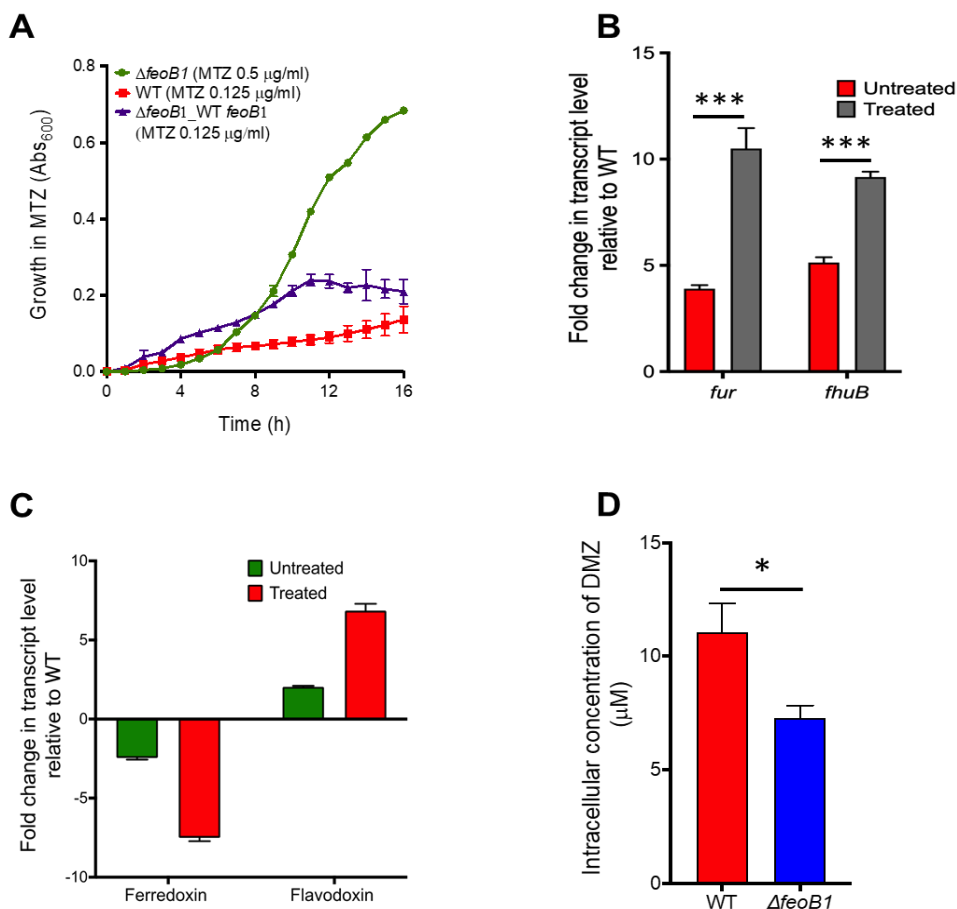
Figure 2. Effect of *feoB1* deletion on: (**A**) growth in metronidazole (MTZ). The Δ*feoB1*

mutant grew better in MTZ, as shown from optical density readings [Abs$_{600}$nm]. MICs

were 1 µg/ml against the Δ*feoB1* mutant and MIC=0.25 µg/ml against the WT and

complemented Δ*feoB1* strains. (**B, C**) Transcription of iron-response genes with respect

to WT strain, in the absence and presence of MTZ at 4 x MIC against each strain.

Increased expression of *fur* and *fhuB* without drug supports iron limitation in Δ*feoB1*

mutant, while expression of flavodoxin over ferredoxin suggests a switch to flavodoxin-

mediated metabolism. (**D**) Intracellular concentration of dimetridazole (DMZ), after 1

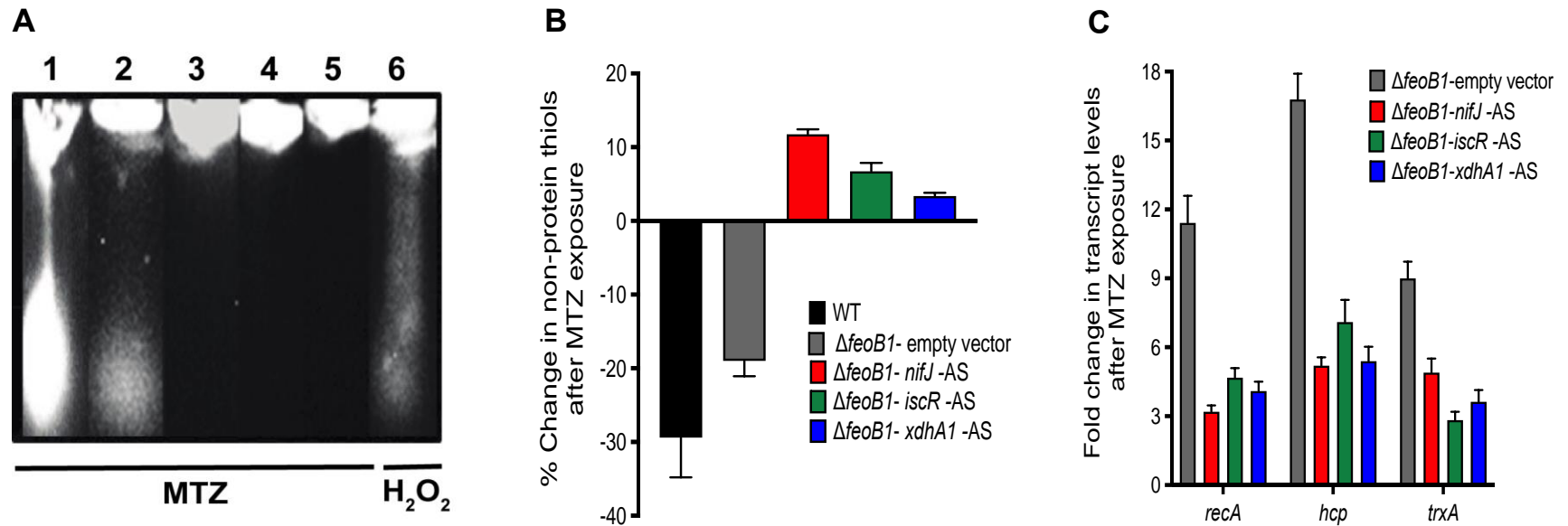hour, in the Δ*feoB1* and WT strains, suggests less drug accumulation in the mutant.

31

664

665

666
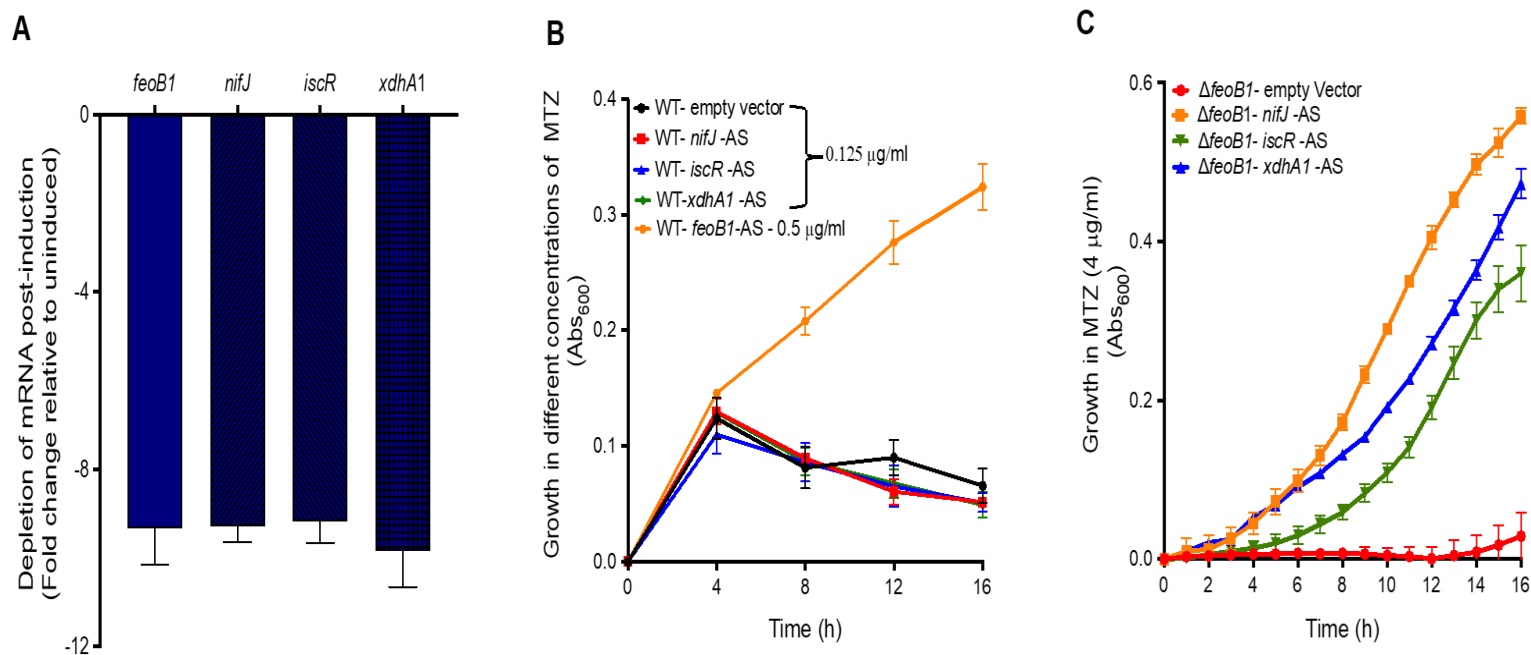
Figure 3. Effect of silencing *nifJ, iscR* or *xdhA1* on resistance in the Δ*feoB1* mutant and WT strain. (**A**) In WT strain depletion of mRNA for *feoB1*, *nifJ, iscR* and *xdhA1* occur when antisenses are induced with xylose (2% w/v); but (**B**) resistance to metronidazole is seen with only depletion of *feoB1* (MIC=1 µg/ml). (**C**) Conversely, in the Δ*feoB1* mutant, expression of either of the three antisenses caused resistance (i.e. MICs of 8 µg/ml versus 1 µg/ml against Δ*feoB1* mutant).

672

A

1 2 3 4 5 6

MTZ H₂O₂

B

% Change in non-protein thiols after MTZ exposure

■ WT
■ ΔfeoB1- empty vector
■ ΔfeoB1- nifJ -AS
■ ΔfeoB1- iscR -AS
■ ΔfeoB1- xdhA1 -AS

C

Fold change in transcript levels after MTZ exposure

■ ΔfeoB1-empty vector
■ ΔfeoB1-nifJ -AS
■ ΔfeoB1-iscR -AS
■ ΔfeoB1-xdhA1 -AS

recA   hcp   trxA

Figure 4. Biochemical and transcriptional validation that higher-level resistance (MIC=8 µg/ml) occurs when mRNA for *nifJ, iscR* or *xdhA1* is depleted in the Δ*feoB1* mutant. (**A**) Metronidazole (MTZ) induced DNA damage was attenuated in the Δ*feoB1* mutant following expression of above antisenses, when compared to Δ*feoB1* and WT strains carrying empty vectors. As a positive control, the WT was exposed to hydrogen peroxide (0.5% v/v) to visualize DNA fragmentation. The image is representative of 3 biological replicates. Resistance was confirmed from there being (**B**) less depletion of non-

681   protein thiols, which form adducts with MTZ; and (**C**) reduced expression of *recA, hcp* and *trxA* that respond to MTZ

682   activity.

683

684

A

B

C
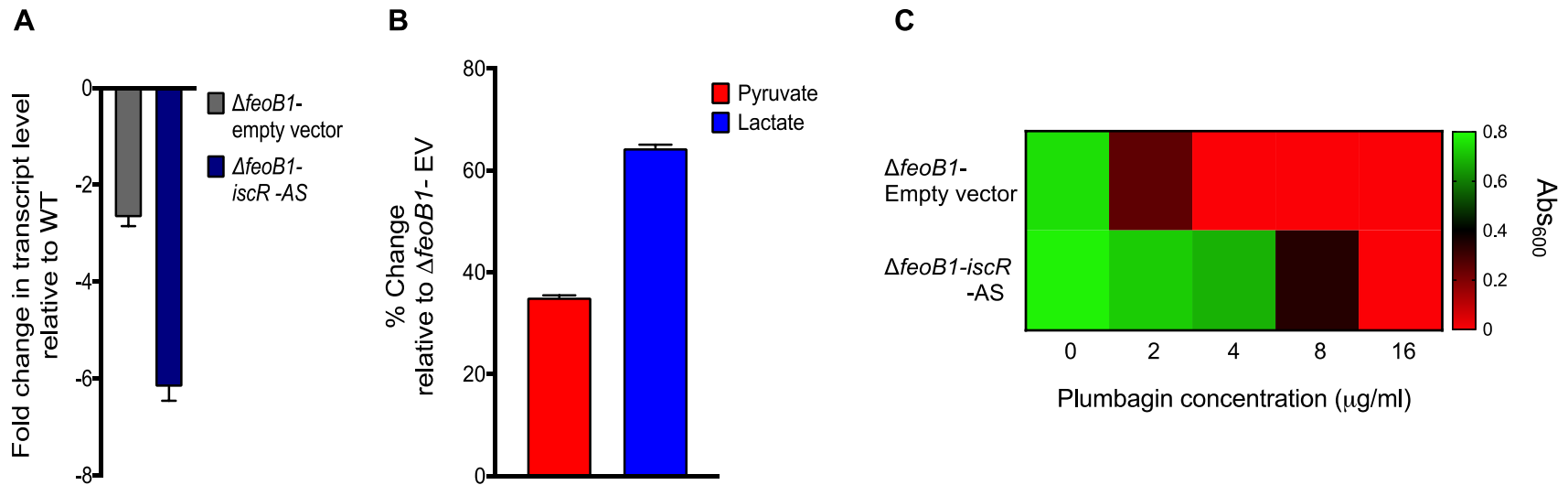
685

686

687   **Figure 5.** Analysis of how *iscR* inactivation promotes metronidazole (MTZ) resistance in the △*feoB1* mutant. (**A**) Depletion

688   of *iscR* mRNA in the △*feoB1* mutant caused further downregulation of *nifJ*, which led to (**B**) accumulation of pyruvate and

689   lactate (all values are relative to △*feoB1*-empty vector). (**C**) Cross-resistance to plumbagin was seen; the heat-map shows

690   that *iscR* depletion enhances growth in plumbagin (like MTZ, plumbagin is an electron acceptor). These results suggest

691   that loss of *iscR* globally affects iron-dependent electron transfer metabolic reactions, including pyruvate-ferredoxin

692   oxidoreductase.

693

694

695
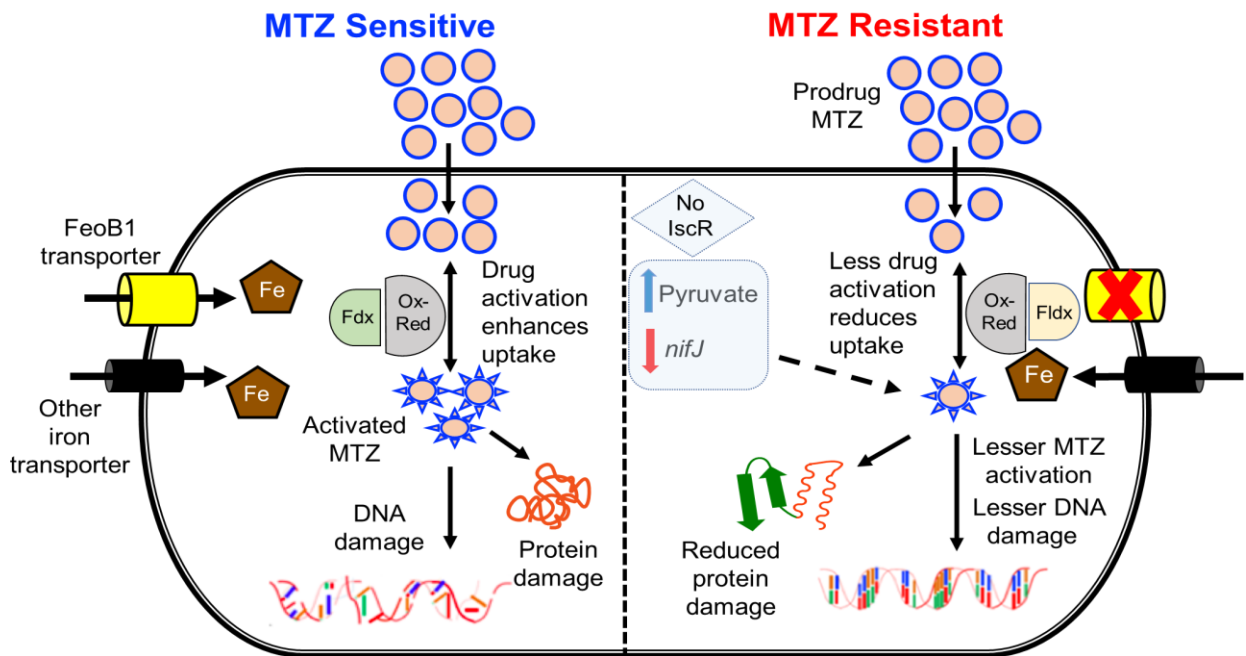
Figure 6. Proposed model of metronidazole (MTZ) resistance in *C. difficile*. (**Left**) In sensitive cells, MTZ is activated by oxidoreductases (Ox-Red; e.g. pyruvate-ferredoxin oxidoreductase [PFOR, *nifJ*]), resulting in free radical damage to DNA and protein damage. Activation then influences drug uptake. Susceptibility is influenced by iron uptake via transporters, mainly FeoB1 (the main iron transporter); and electron carrier proteins ferredoxin (Fdx) with low redox potential. (**Right**) In MTZ-resistant cells, loss of FeoB1 decreases intracellular iron content, probably shifting cells from ferredoxin (Fdx) to flavodoxin (Fldx) mediated metabolism. Fldx is less effective in activating MTZ. Loss of *iscR* synergizes with defective *feoB1* to further reduce metabolic activities that activates MTZ.